Visualization of Internal Flow Dynamics in Counterflow Atomizers Using X-Ray Diagnostics and Laser Shadowgraphy

A. Hoxie[1], V. Srinivasan[2], E. Johnson[2], A. Kastengren[3]
University of Minnesota, Duluth
University of Minnesota, Twin Cities
Argonne National Laboratory

Abstract

Experiments were carried out to observe the flow inside counterflow atomizers over a range of operating conditions and fluid properties. Liquids used were water and propylene glycol, while the gas was either air or helium. Liquid flow rates ranged from 10 ml/min to 40 ml/min, with gas liquid ratio (GLR) ranging from 0.1 to 0.6. The primary experiments used the 7-BM line of the Advanced Photon Source in Argonne National Laboratories with a 2.6 mm atomizer produced from (Poly)Ethyl-Ether-Ketone (PEEK). The X-Ray beam was operated in phase contrast mode, leading to interference patterns near the gas-liquid interface and enabling a qualitative understanding of the flow structure. Complementary optical work applied laser shadowgraphy to a 1 mm orifice atomizer constructed with quartz capillary tubing. A diffuse pulsed Nd:YAG laser backlight captured instantaneous gas-liquid interface positions in the internal flow. With both techniques, two distinct flow behaviors are observed corresponding to low and high GLR values. At low GLR, the inertia of the injected gas is insufficient to penetrate the liquid downflow. The gas stream entering the mixing chamber in the upstream direction is immediately deflected by the denser liquid and enters the discharge tube around a central liquid jet, which is sheared and accelerated by the surrounding gas, leading to breakup. A distinct frequency of jet breakup is observed inside the discharge tube, with the liquid jet oscillating and fragmenting against the walls. The situation at high GLR is quite different, however, as the incoming gas stream asymmetrically penetrates upstream into the mixing chamber, taking the form of a high-speed jet confined along one wall, and displaying a flapping instability as it encounters the liquid flowing downstream. This flapping causes violent mixing, resulting in a highly disturbed interface, along with the generation of liquid ligaments and gas bubbles. This two-phase mixture enters the discharge tube with no liquid jet formation evident for this case. The transition between these two regimes is explored by changing the liquid viscosity and gas molar mass, and weak sensitivity to fluid properties is observed. Further, quantitative image analysis techniques applied to the low and high GLR cases allow extraction of the frequencies of the liquid jet in the discharge tube at low GLR, as well as the flapping mode at high GLR.

*Corresponding author: vinods@umn.edu

Introduction

Atomization of viscous liquids is an ubiquitous process in industry, incurring in diverse applications such as spray painting, dust control, spray drying, and snow making. In all these processes, the ability to control the droplet diameter distribution is critical to product and process quality. Conventional external mixing designs such as pressure-swirl injectors and air-blast atomizers use the relative velocity between liquid and gas to overcome surface tension and promote the growth of instabilities, which leads to primary atomization, and far downstream, secondary atomization of droplets under aerodynamic forces [1]. This approach yields diminishing returns when the liquid viscosity increases substantially relative to liquids such as water, resulting in large droplets or incomplete atomization.

Recently, a new type of internal mixing nozzle, the Counterflow (CF) nozzle, has been developed and tested under a wide range of operating conditions [2]. This nozzle has a novel geometry, whose flow passages are configured such that liquid and gas streams interact inside the nozzle in a countercurrent flow configuration. The hypothesis used to design this configuration was that in single-phase flows, such countercurrent flow configurations are known to establish regimes of high turbulent mixing, with the transport occurring due to turbulent rather than viscous mean stresses, thereby rendering the variation of viscosity less important. The performance curves of the CF have been documented in a few recent articles [3-5]. The nozzle is an internal mixing design that shares some similarities with effervescent atomization [6] and flow-blurring [7] designs; however, unlike effervescent atomization, there does not appear to be an upper bound on the Gas-Liquid Ratio (GLR), and unlike flow-blurring, all the atomizing gas first interacts with liquid inside the nozzle. The major observations that can be made are: (a) the emergence of the liquid as a nearly fully atomized spray in the near-field, with weak secondary atomization, (b) high operating efficiency (defined in terms of surface area created per unit energy input), (c) the ability to produce fine droplets with mean droplet diameters less than 45 microns from liquids as viscous as 500 cP, and (d) the reduction of droplet diameter as the molecular weight of the atomizing gas is reduced. A preliminary model [4] that assumes the formation of a well-mixed two-phase mixture inside the mixing chamber of the nozzle, combined with assumed scalings for the dimensions of bubbles introduced into the mixing chamber, was able to partially explain the collapse of data [ref].

However, such modeling efforts are based on the observed droplet diameter distributions in the far field of the spray, and not through any direct visualization of the flow inside the nozzle. Moreover, some observations in the droplet mean diameter, such as a sharp reduction beyond a certain value of injected gas mass flow rate [5], cannot be explained by this model. This model was originally based on data obtained with water; however, experiments with more viscous liquids show greater deviation from the model. Scaling up the geometry is unlikely to yield improved visualization using conventional techniques based on monochromatic optical light sheets, since the formation of a two-phase mixture inside the nozzle creates a high density of liquid-gas interfacial area, causing multiple scattering events for any light beam passing through. Therefore, we explore an alternate technique for visualization, namely the use of C-Ray diagnostics to obtain patterns that elucidate the transmission and absorption of radiation due to the arrangement of liquid and gas inside the nozzle.

The objectives of this study are to visualize and understand the flow dynamics inside the CF nozzle, as a function of liquid and gas flow rates, gas density (controlled independently of molar mass through different gases), and liquid viscos-

ity. Recent developments in advanced X-Ray diagnostics, such as X-Ray Phase Contrast Interferometry and X-Ray Fluorescence Spectroscopy lend themselves to qualitative and quantitative understanding of dense gas-liquid flows. In the present study, XPCI is used for qualitative understanding.

Experiments

The 7-BM-B line of the Advanced Photon Source (APS) of the Argonne National Laboratory was used for this study. In this beamline, a synchrotron bending magnet acts on an electron beam, producing a collimated, broadband X-Ray beam which enters the test chamber. Details of the X-Ray beam quality and characterization can be found in ref. [8]. The CF nozzle is mounted on a motorized traverse and placed in the path of the X-Ray bean. The intensity of an X-Ray beam is attenuated to different extents, depending upon the wavelengths of the beam and the molecular structure of the medium through which it passes, thus providing a contrast between liquid and gas. The XPCI technique (Fig. 1) yields qualitative information about the instantaneous density field. The incident X-Ray has higher energy, is polychromatic, and is in the form of an extended beam, providing a large field of view rather than a point measurement. X-Rays are weakly refracted by the three-dimensional phase boundaries between solid, liquid and gas. As the refracted waves propagate, interference occurs, with the interference pattern sensitive to the density gradients rather than the absolute value of density [9]. The interference pattern is formed on a scintillator which converts it to a visual image. A high-speed camera captures images with a resolution of 10.5 μm per pixel. Quantitative measurements of the beam path-averaged density using X-Ray Fluorescence Spectroscopy [10, 11] are planned for a future study.

The CF nozzle placed in the path of the beam was made of (poly) ethyl-ether-ketone (PEEK), a plastic that has high structural rigidity and can handle internal pressures ~ 5 bar while offering significant transmissivity to X-Rays. Figure 2 shows the internal geometry of the CF nozzle used. Liquid from a pressurized reservoir flows through a mass flow controller to the core passage (diameter, d_2) of the nozzle, while gas is supplied to the annular space in the nozzle. The gas flows coaxially in the annular space, before turning by 180°, flowing upstream around the discharge tube of outside diameter d_1 and encountering the oncoming liquid stream. The countercurrent flow configuration establishes high turbulence levels and strong mixing, presumably creating a two-phase mixture in the mixing chamber (the near-tip region of the liquid tube), which is imaged using the X-Ray beam. This two-phase mixture exits the nozzle through the discharge tube of diameter d_0. The relevant dimensions of the CF nozzle are enlisted in Table 1.

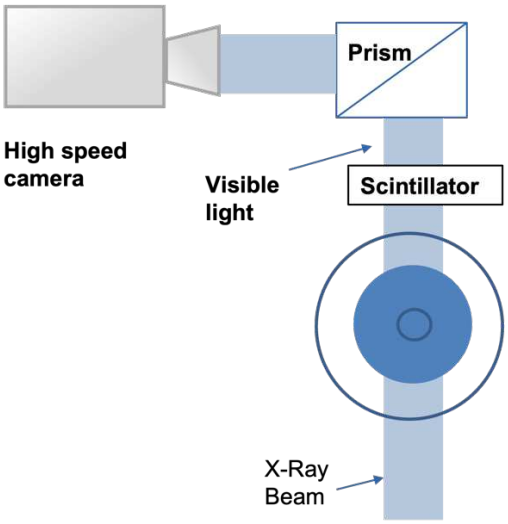

Figure 1. Schematic diagram of the X-Ray Phase Contrast Interferometry setup.

Two liquids --- water and propylene glycol (PG) were tested at multiple flow rates ranging from 10 ml/min to 60 ml/min. The gas mass flow rates expressed non-dimensionally as a Gas-Liquid Ratio (GLR) was varied from 0.03 to 0.6. The properties of the liquids used are listed in Table 2.

For each test condition specified by liquid and gas mass flow rates, liquid properties, and spatial location being imaged, images were taken at 5000 frames per second for 4 seconds. The gray-scale images are the result of absorption of X-Ray radiation by the two-phase mixture in the nozzle, as well as the PEEK walls of the nozzle. Therefore, reference images were taken at each position of the nozzle in the beam path, that were used to normalize the images with the flow. This resulted in a set of normalized images whose pixel values nominally represent the attenuation of the beam through the beam path.

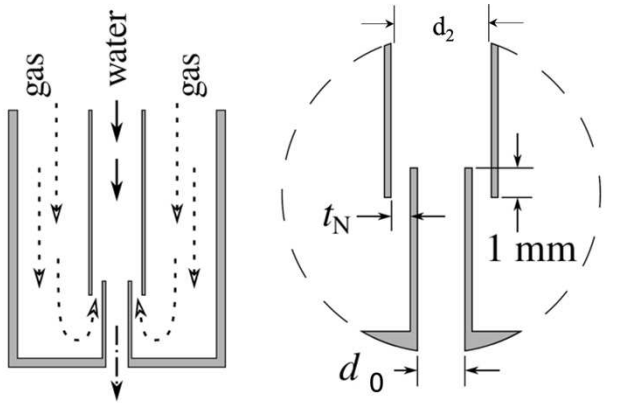

Figure 2. Sketch of the Counterflow nozzle.

Table 1. Values of important dimensions (mm) in the CF nozzle.

d_o	d_1	d_2	L
1.6	2.2	2.6	1

Table 2. Physical properties of liquids used in study.

Fluid	**Density (kg/m^3)**	**Surface Tension (N/m)**	**Viscosity (mPa.s)**
Water	998	0.07	0.89
Propylene glycol	1042	0.04	49.3

Results

The raw images were adjusted in the software NIH-ImageJ to enhance contrast and elucidate flow features. This process also accentuates the vignetting and absorption effect inherent in the optical setup, leading to dark horizontal bands at the top and bottom of each image. For assistance in interpretation of subsequent figures, Figure 3 shows the geometry sketch superimposed on an actual X-Ray image. The liquid enters from the top, the gas enters from the bottom on the sides (the annular region) and the discharge tube wall shows up as two rectangular posts (hatched in the figure). The opaque rectangular region at the bottom corresponds to a PEEK piece used to fix the discharge tube to the nozzle housing. The bottom plane of this piece is the exit plane of the nozzle discharge.

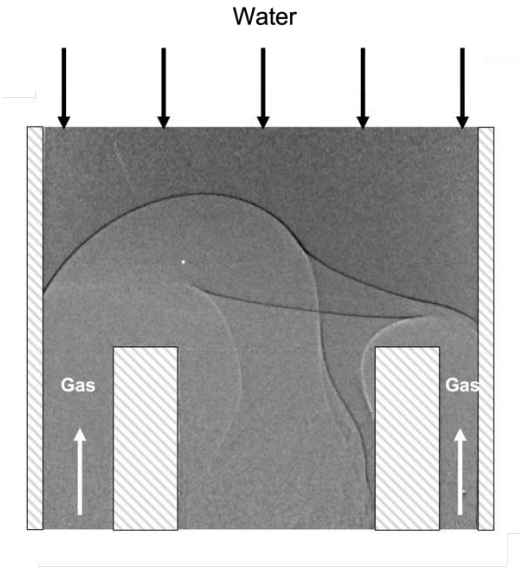

Figure 3. Representative image from measurements along with superimposed geometry, for aid in interpretation.

Figure 4 shows a composite image created by stitching two images taken at different axial locations and at different times. These images were taken for operating conditions defined by a water flow rate of 40 ml/min, and an atomizing air flow adjusted to yield a high value of GLR= 0.59. It is apparent that the gas enters the mixing chamber along the periphery as a high-speed jet with significant momentum, penetrating far upstream into the liquid. The jet curves away from the wall due to the pressure of oncoming liquid and undergoes breakup through an apparent shear-driven flapping instability.

The breakup of the gas jet generates gas bubbles and liquid ligaments of multiple scales that can be observed in the upstream region. The gas bubbles can penetrate as far upstream as 6 mm (note the discharge tube diameter of 1.6 mm at the bottom of the lowermost image). The breakdown of the gas jet and consequent formation of liquid ligaments appears responsible for no clear contrast between liquid and gas in the flow entering the discharge tube, suggesting the two phases are well mixed at the entrance.

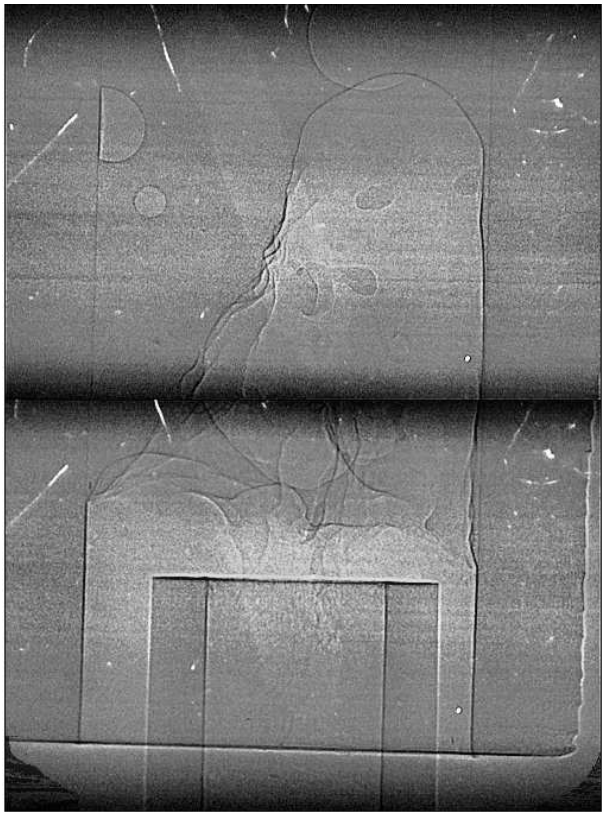

Figure 4. Composite image showing the flow structure for a water flow rate of 40 ml/min and GLR=0.59.

Figure 5 shows the corresponding images for the same liquid flow rate but a reduced GLR = 0.3. It is apparent that the reduction in GLR substantially reduces the momentum of the gas jet, and it does not penetrate far into the liquid, or undergo shear-driven breakup. Instead, the gas jet undergoes turning almost immediately after entering the liquid tube, under the action of the oncoming liquid, and enters the discharge tube along with the liquid. A steady separation bubble of gas is formed on the flat surface of the end of the discharge tube, attesting to the relative quiescence of the flow. While some large bubbles are visible, the liquid, does not undergo any significant breakup, and no ligaments are visible in the mixing chamber. Instead, the liquid enters the discharge tube as a clearly visible coherent stream in the core, with the gas flowing coaxially in the annular space between the liquid and the wall of the discharge tube. The acceleration of the gas due to the reduced cross-section promotes the growth of Kelvin-Helmholtz instabilities on the liquid surface. In videos, the liquid is seen to behave like a jet undergoing pinch off; large ligaments are seen to break off under the action of the gas shear inside the discharge tube and the flow is extremely unsteady, despite the relative steadiness of the entrance flow.

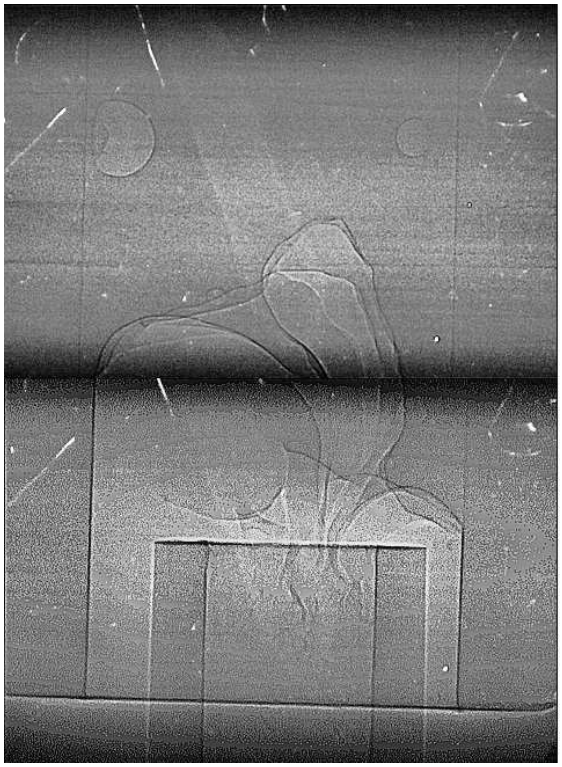

Figure 5. A composite image depicting the flow structure for a water (40 ml/min) and GLR=0.3

The behaviors observed by X-Ray in Figs. 4-5 were also observed using visible 532 nm light in complementary images of a similar CF atomizer constructed of quartz capillary tubing (d_0, d_1, d_2 = 1.0, 1.2, 1.5 mm, L = 1 mm). A diffuse pulsed Nd:YAG laser backlight allowed <10 ns effective exposure time in Figure 6, showing instantaneous air-water interface positions at (from left to right) GLRs of 0.22, 0.36, and 0.83. It can be seen that gas penetrates farther upstream at larger GLR, with asymmetry and perturbation of the interface increasing significantly at higher GLR. Small bubbles and pockets are located on the interface near the injection region in all cases, while farther upstream interfaces show less perturbation and larger bubbles remain almost spherical.

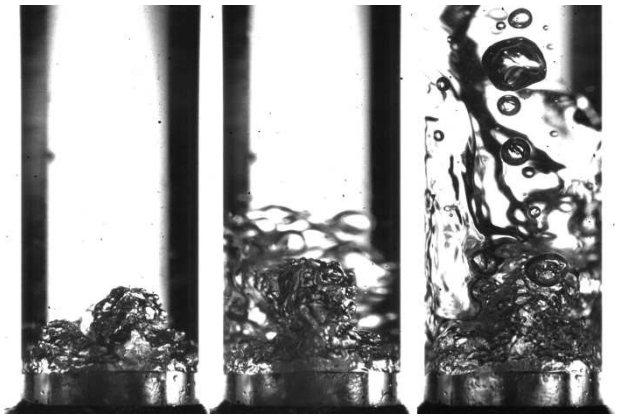

Figure 6. Images of the injection region using diffuse visible light pulse of <10 ns, with (from left to right) GLR of 0.22, 0.36, and 0.83.

Figure 7 shows corresponding images with helium as the atomizing gas. The water flow rate used was kept equal to approximately 40 ml/min, but the gas flow rate was adjusted to much lower values of GLR= 0.08. This was motivated by previous work that suggested that much lower GLR values are required to achieve the same Sauter Mean Diameters in the spray when low molecular weight gases are used. Despite this significantly lower GLR, it is apparent that the overall flow structure is like that of the high-GLR condition encountered with air as the atomizing gas, shown previously in Fig. 3. While the penetration of the gas stream into the liquid tube is not as evident as for air in Fig. 3, large bubbles are visible, and the flow in the discharge tube seems well mixed with no sharp interface as is true in Fig. 4.

Figure 8 compares representative images taken near the entrance to the discharge tube for high, moderate, and low values of GLR with helium. It is apparent that as GLR is reduced to the smallest value of GLR= 0.02, the flow structure is like that encountered for air/water flows with a GLR of 0.3. The entering gas flow immediately turns around towards the discharge tube, with the sharpness of the curved interface attesting to the steady nature of the flow. The two fluids do not mix in the mixing chamber, enter the discharge tube as coherent streams, where the onset of Kelvin-Helmholtz instabilities derived liquid ligament formation. At high GLR, the phase interface along the curved gas path appears more diffuse, suggesting more vigorous mixing. At the intermediate GLR value of 0.04, the situation appears to be closer to the low GLR situation, with a well-defined carved interface and a clear core of liquid entering the discharge tube, suggesting that the transition in flow character occurs between GLR=0.04 and GLR=0.08.

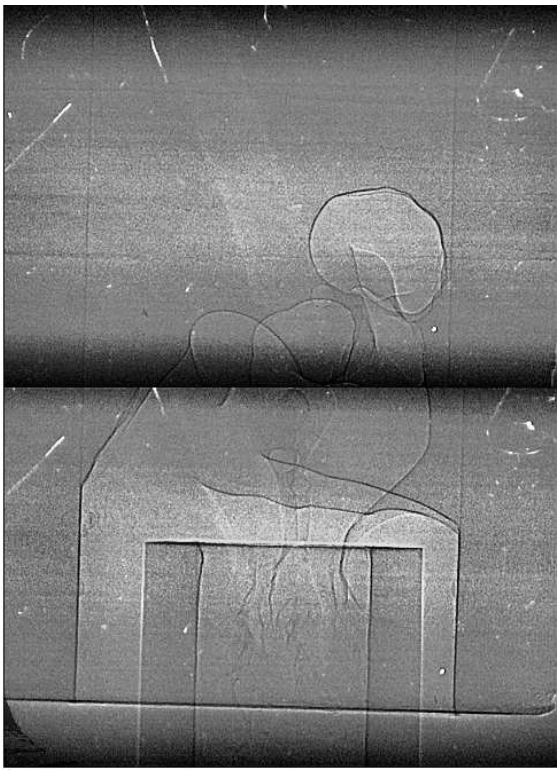

Figure 7. Flow structure inside the nozzle for water flowing at 40 ml/min and helium flow rate yielding GLR=0.08.

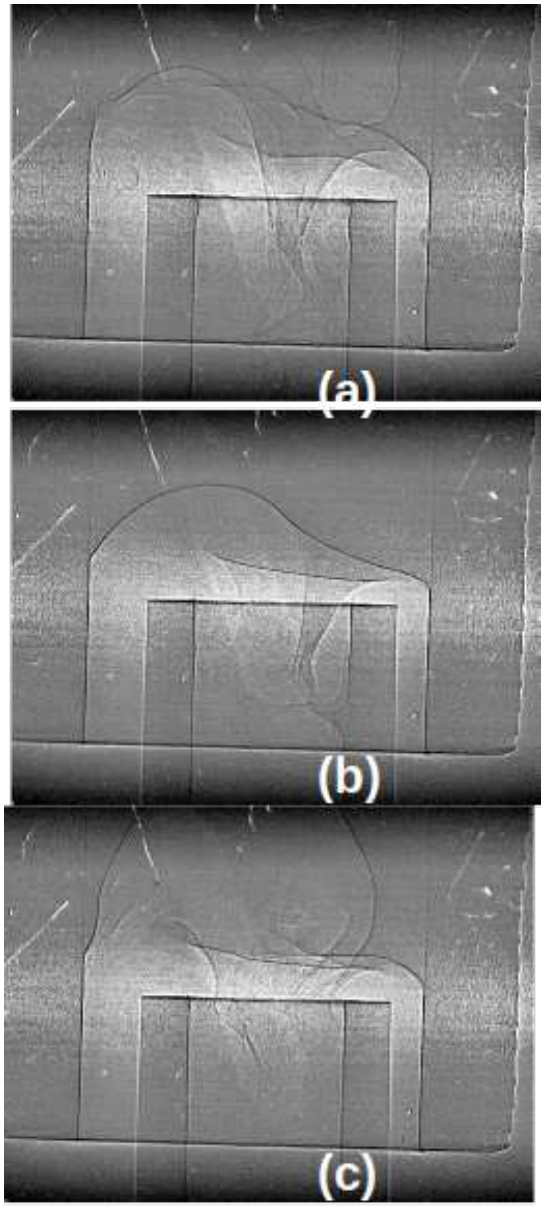

Figure 8. Comparison of flow structures inside the nozzle for low, moderate, and high GLR, with water as liquid and helium as atomizing gas. (a) GLR=0.08 (b) GLR = 0.04 (c) GLR = 0.02.

Figure 9 depicts the phase interface at multiple values of water flow rate: 19, 40, 92 and 130 ml/min. The corresponding GLR values were 0.6, 0.6, 0.51 and 0.46, with the GLR value at the highest liquid flow rate being lower due to facility limitations. All these test conditions are

expected to correspond to the regime of turbulent mixing in the mixing chamber. Looking at the images, no major differences are perceptible, suggesting that the mixing process is more sensitive to GLR and less sensitive to absolute values of the liquid or gas flow rates for a given liquid/gas combination. Some difference is evident when comparing the smallest and largest flow rates, however; the phase interface seems more well-defined and steadier in the region immediately above the entrance to the discharge tube for the lowest mass flow rate, when compared to the highest mass flow rate, where a multiplicity of wrinkled phase interference lines suggests greater mixing.

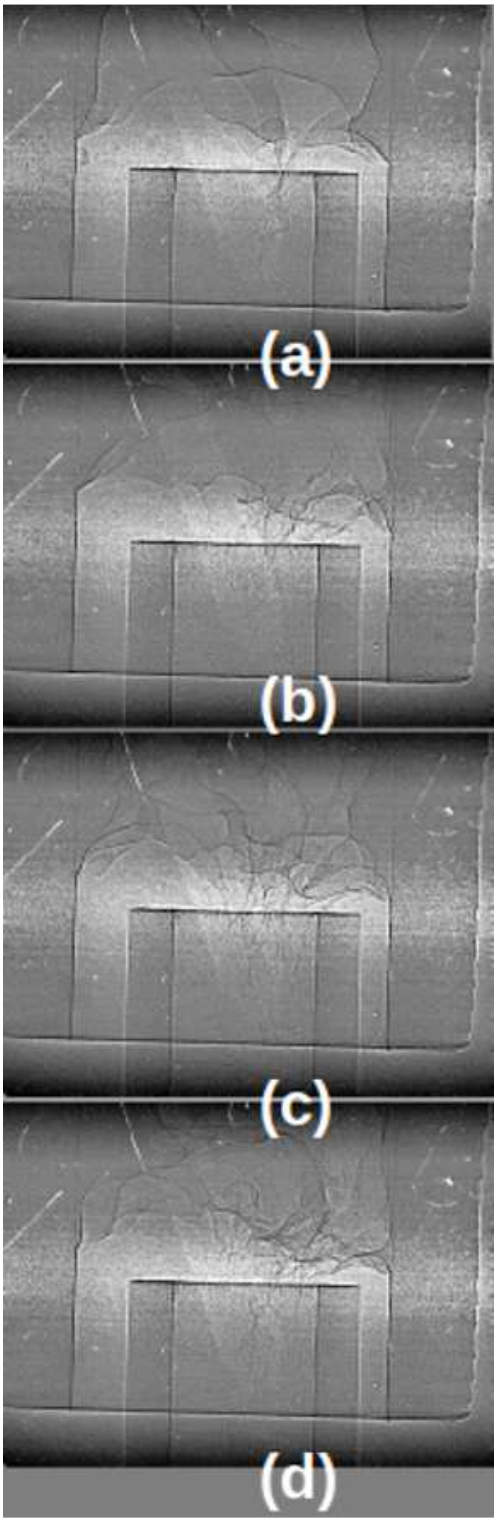

Figure 9. Flow visualization inside the nozzle for various liquid flow rates and GLR: (a) 19 ml/min, GLR=0.59 (b) 40 ml/min, G:R=0.59

(c) 92 ml/min, GLR=0.51 (d) 130 ml/min, GLR=0.45.

With the understanding that the flow structure is relatively insensitive to the magnitude of flow rate at constant GLR, we are now able to examine the effects of GLR in greater detail. Figure 10 examines the flow near the entrance to the discharge tube as a function of the gas-liquid mass flow ratio GLR. Figures 3 and 4 suggest that there are two distinct regimes in the flow. We now attempt to narrow the transition boundary by considering five different conditions shown in Fig. 8 with GLR ranging from to 0.59. For the low GLR values ranging from 0.13 to 0.26, the liquid core in the discharge tube is readily apparent. This core appears mixed out at GLR=0.39, and is not visible at GLR=0.59, suggesting that the transition value of GLR for the air-water combination is between 0.39 and 0.6. This may explain the results of Rangarajan and Srinivasan [4] who found little variation in mean droplet diameter for this nozzle geometry until the GLR was increased beyond 0.5.

Figure 11 considers the effects of liquid viscosity. As seen in Table 2, propylene glycol is 45 times more viscous than water, with the result that Reynolds numbers describing the flow are significantly lower for the same volumetric flow rates. At low or moderate GLR, the flow structure is like that for water, with the fragmentation of the liquid core occurring in the discharge tube. Mixing in the chamber prior to entry into the discharge tube only occurs at higher GLR.

It is apparent that while the increase in GLR causes this transition from the low-GLR regime (jet breakup in the discharge tube) to the high GLR regime (bulk mixing in the liquid tube due to gas jet breakup), the exact value of GLR at which this transitions a function of liquid viscosity.

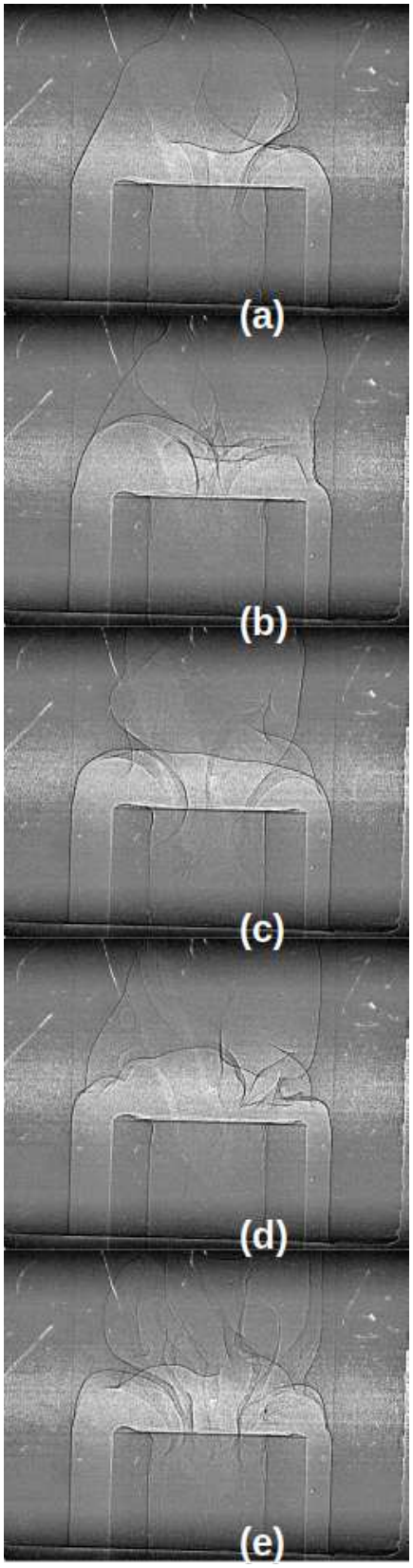

Figure 10. Effects of variation in GLR on flow structure. (a) Ql= 92 m;/min. GLR=0.13

(b) Ql = 48 ml/min, GLR=0.18 (c) Ql = 35 ml/min, GLR =0.26 (d) Ql= 45.5 ml/min, GLR=0.39 (e) Ql = 40 ml/min. GLR=0.59.

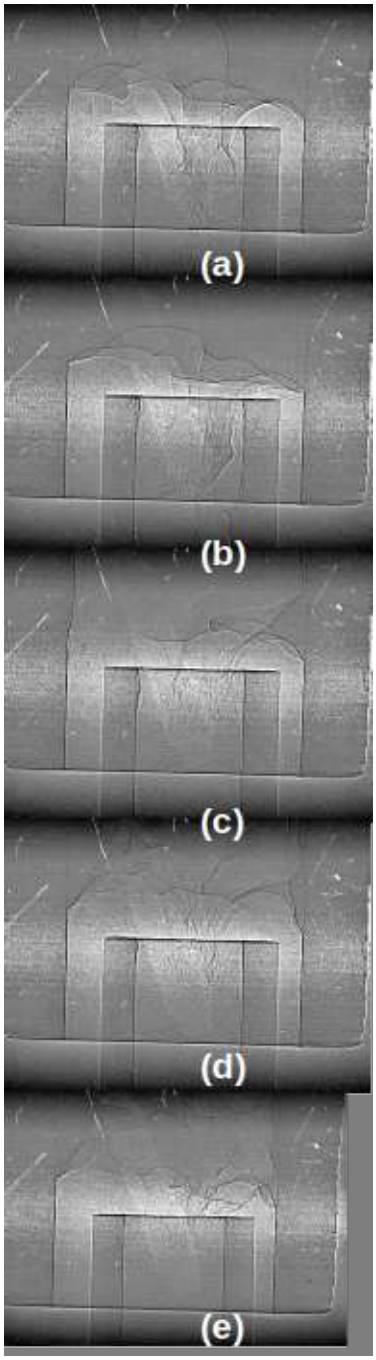

Figure 11. Effect of liquid viscosity on the flow structure (a) PG at GLR=03. ;(b) PG at GLR=0.33; (c) PG at GLR=0.59; PG at GLR=0.89 (d)PG at GLR=1.18.

To extract more quantitative information from these images, we consider that the greyscale values in these images represent the degree of transmission through the fluid, which, with knowledge of the gas and liquid density values, is equivalent to the volume fraction. If the incident X-Ray bean has intensity I_0, then the intensity incident on the detector after passing through nozzle wall and fluid is

$$I_1 = I_o e^{(a_{\lambda p} L_p + a_{\lambda l} L_l + a_{\lambda g} L_g)} \quad (1)$$

where subscripts p, l, g refers to plastic, liquid, and gas respectively, and the constants a_λ refer to their respective absorption coefficients. If another measurement is made in which there is no gas or liquid flow and yields an intensity I_2:

$$I_2 = I_o e^{(a_{\lambda p} L_p)} \quad (2)$$

If we assume a spectrally narrow beam, we can write for the transmission ratio:

$$\tau = \frac{I_1}{I_2} = e^{-(a_p L_p + a_g L_g)} \quad (3)$$

This quantity can be constructed by analyzing images taken with and without flow and is expected to yield values less than 1 everywhere in the domain.

However, the phase interference at the gas-liquid interface boundaries can cause the values of this quantity to be greater than 1. Therefore, despite the potential to extract quantitative information, we refrain from calculating beam path-averaged void fractions. However, there remains an opportunity to calculate the flapping frequency of the gas shear layer at high GLR, and the jet breakup frequency in the discharge tube at low GLR. This is accomplished by sampling one pixel value (corresponding to a fixed spatial location) across 4000 successive images and constructing a time series for that spatial location. A Fast Fourier Transform of that time series yields the frequency spectrum of transmission at that location, which may potentially reflect the oscillatory frequency of the gas shear layer/phase interface as it crosses the sampling location.

Figure 12 shows such a frequency spectrum for the case of water sprayed at 40 ml/min with He

as the atomizing gas with GLR=0.04. A sharp frequency peak at 230 Hz is apparent with amplitude well above the background noise, along with a harmonic at 460 Hz. These frequencies differ by about 30% from the frequencies calculated in [Rangarajan2020] for the case of water and air. Such spectra emerge at multiple sampling locations in the central region of the discharge tube, with no change in the locations of the frequency peaks, strongly suggesting that the K-H instability is indeed responsible for the fluctuation in transmissivity.

The high-GLR regime is characterized by the penetration of the gas stream into the mixing chamber, and the instability of this gas stream as it breaks down and mixes with the liquid. Despite visual evidence of the gas stream flapping and breaking down, a spectrum obtained for the high-GLR regime, at a location in the near-wall region of the liquid tube/mixing chamber (Fig. 13) shows no evidence of frequency peaks. In fact, the log-scale plot of the fluctuations shows a strong power-law roll off behavior, suggesting that the intense mixing sets up broadband turbulence over a large range of length and time scales.

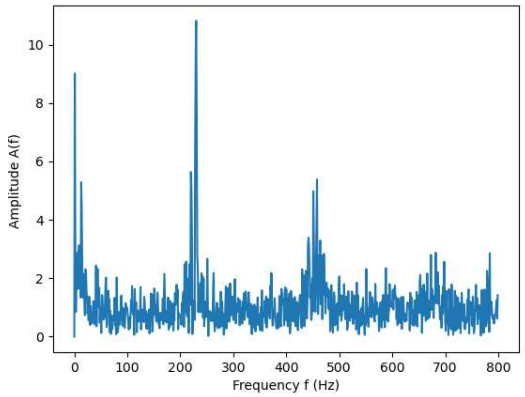

Figure 12. Frequency spectrum of fluctuations in pixel value in the discharge tube for a water flow rate of 45 ml/min, GLR=0.04 and He as the atomizing gas.

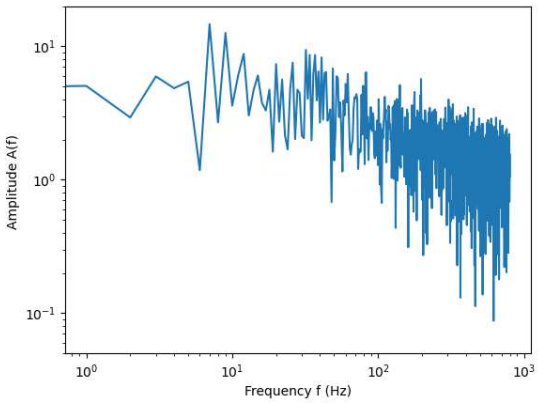

Figure 13. Log-plot of frequency spectrum of fluctuations in pixel value in the mixing chamber for a water flow rate of 45 ml/min, GLR=0.6 and air as the atomizing gas.

Summary

Qualitative observations of the dynamics of the internal flow fields inside a Counterflow nozzle were made using X-Ray Phase Contrast Imaging radiography. The results strongly suggest two distinct modes of breakdown of flow that likely determine the previously documented external flow behavior. For a given gas-liquid combination, the flow at low GLR is marked by negligible mixing inside the liquid tube, with most of the liquid fragmentation occurring in the discharge tube through a confined Kelvin-Helmholtz type instability. At high GLR, the gas stream entering the mixing chamber has sufficiently high momentum that it penetrates substantially upstream, undergoes a shear-driven breakup, and creates a two-phase mixture, which enters the discharge tube. These breakup modes carry distinct signatures in their spectral content and can be detected from analysis of the transmitted intensity. The transition between these modes occurs at or near a vertical value of GLR that is dependent on the liquid and gas properties; decreasing as gas density is reduced and increasing with liquid viscosity. Over the range of conditions studied, the value of transition GLR

does not seem to substantially depend on the magnitude of liquid flow rate.

Acknowledgements

This research used resources of the Advanced Photon Source, a U.S. Department of Energy (DOE) Office of Science user facility operated for the DOE Office of Science by Argonne National Laboratory under Contract No. DE-AC02-06CH11357.

Researchers from the University of Minnesota were supported by a grant (CBET-2023932) from the National Science Foundation.

References

1. Lefebvre, A.H. and McDonell, V.G., 2017. *Atomization and sprays*. CRC Press.
2. Hoxie, A., E. Johnson, V. Srinivasan, and P. J. Strykowski. 2018. "Characterization of a Novel Energy Efficient Atomizer Employing Countercurrent Shear." In *The 14th International Conference on Liquid Atomization and Spray Systems*, 1–9. Chicago. USA: 22-26 July, 2018.
3. Johnson, E. J., V. Srinivasan, P. J. Strykowski, and A. Hoxie, "Influence of Injection Gas Molar Mass on Counterflow Atomizer Performance", Atomization and Sprays, In Press.
4. Rangarajan, R., and V. Srinivasan. 2022. "Enhanced Atomization of Viscous Liquids Using a Counterflow Nozzle." *Atomization and Sprays*
5. *Rangarajan, R., H. Zhang, P. J. Strykowski, A. Hoxie, S. Yang, and V. Srinivasan. 2020. "Atomization of High Viscosity Liquids Using a Two-Fluid Counterflow Nozzle: Experiments and Modeling." In ASME Turbo Expoo, GT2020-15691. London, UK.*
6. *Sovani, S.D., Sojka, P.E. and Lefebvre, A.H., 2001. Effervescent atomization. Progress in energy and combustion science, 27(4), pp.483-521.*
7. *Gañán-Calvo, A.M., 2005. Enhanced liquid atomization: From flow-focusing to flow-blurring. Applied Physics Letters, 86(21), p.214101.*
8. *Kastengren, A.L., Powell, C.F., Arms, D., Dufresne, E.M. and Wang, J., 2010, May. Spray diagnostics at the advanced photon source 7-bm beamline. In ILASS Americas, 22nd annual conference on liquid atomization and spray systems, Cincinnati, OH.*
9. *Duke, D., Swantek, A., Kastengren, A., Fezzaa, K. and Powell, C., 2015. Recent developments in X-ray diagnostics for cavitation. SAE International Journal of Fuels and Lubricants, 8(1), pp.135-146.*
10. *Duke, D.J., Kastengren, A.L., Matusik, K.E. and Powell, C.F., 2018. Hard X-ray fluorescence spectroscopy of high pressure cavitating fluids in aluminum nozzles. International Journal of Multiphase Flow, 108, pp.69-79.*
11. *Lin, K.C., Kastengren, A., Bornhoft, B. and Carter, C.D., 2018. Derivations of Averaged Two-Phase Flow Properties Using X-Ray Fluorescence Measurements. In 2018 AIAA Aerospace Sciences Meeting (p. 1547).*